Analytical ultracentrifugation

Patel, Trushar R.; Winzor, Donald J.; Scott, D

DOI:
10.1016/j.ymeth.2015.11.006

Document Version
Peer reviewed version

Citation for published version (Harvard):
Patel, TR, Winzor, DJ & Scott, D 2016, 'Analytical ultracentrifugation: a versatile tool for the characterisation of macromolecular complexes in solution', *Methods*, vol. 95, pp. 55-61. https://doi.org/10.1016/j.ymeth.2015.11.006

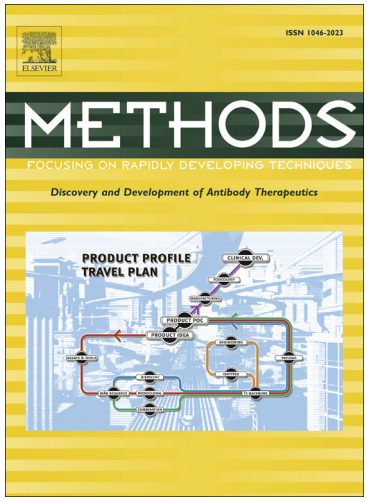

Analytical ultracentrifugation: A versatile tool for the characterisation of macromolecular complexes in solution

Trushar R. Patel, Donald J. Winzor, David J. Scott

PII: S1046-2023(15)30145-6
DOI: http://dx.doi.org/10.1016/j.ymeth.2015.11.006
Reference: YMETH 3838

To appear in: *Methods*

Received Date: 17 September 2015
Revised Date: 5 November 2015
Accepted Date: 7 November 2015

Please cite this article as: T.R. Patel, D.J. Winzor, D.J. Scott, Analytical ultracentrifugation: A versatile tool for the characterisation of macromolecular complexes in solution, *Methods* (2015), doi: http://dx.doi.org/10.1016/j.ymeth.2015.11.006

METHODS–D–15–00214R1

Analytical ultracentrifugation: A versatile tool for the characterisation of macromolecular complexes in solution

Trushar R. Patel[a*], Donald J. Winzor[b] and David J. Scott[c,d,*]

[a]*School of Biosciences, University of Birmingham, Edgbaston, B15 2TT United Kingdom*

[b]*School of Chemistry and Molecular Biosciences, University of Queensland, Brisbane, Queensland 4072, Australia*

[c]*National Centre for Macromolecular Hydrodynamics, School of Biosciences, University of Nottingham, Sutton Bonington Campus, LE12 5RD, United Kingdom*

[d]*ISIS Spallation Neutron and Muon Source and Research Complex at Harwell, Rutherford Appleton Laboratory, Oxfordshire OX11 0FA, United Kingdom*

---

*Corresponding authors.

Trushar R. Patel (trushar7@hotmail.com), David J. Scott, (David.Scott@nottingham.ac.uk)

Highlights:

- Application of analytical ultracentrifuge to study macromolecular assemblies
- Sedimentation velocity analysis to assess quality of reconstituted cytoplasmic dynein (CyDn) complex
- Sedimentation velocity and equilibrium analysis to justify monomeric nature of activated ERK2
- Comparison of crystal structure of $tRNA^{Sec}$–SepSecS complex with its solution state using sedimentation velocity analysis

Abstract

Analytical ultracentrifugation, an early technique developed for characterizing quantitatively the solution properties of macromolecules, remains a powerful aid to structural biologists in their quest to understand the formation of biologically important protein complexes at the molecular level. Treatment of the basic tenets of the sedimentation velocity and sedimentation equilibrium variants of analytical ultracentrifugation is followed by considerations of the roles that it, in conjunction with other physicochemical procedures, has played in resolving problems encountered in the delineation of complex formation for three biological systems – the cytoplasmic dynein complex, mitogen-activated protein kinase (ERK2) self-interaction, and the terminal catalytic complex in selenocysteine synthesis.

Keywords:

Analytical ultracentrifugation

Catalytic complex in selenocysteine synthesis

Cytoplasmic dynein complex

Mitogen-activated protein kinase (ERK2)

Sedimentation equilibrium and

Sedimentation velocity

SepSecS–tRNA^{Sec} interaction

1. Introduction

Although proteins can be isolated from biological extracts, their roles *in vivo* usually entail involvement in larger complexes and/or networks of proteins that interact with each other. There is therefore great interest in the characterization of these complexes and interactions that is essential to a complete understanding of their biological function at the molecular level. Quantitative studies of proteins and their interactions stem from the development of an ultracentrifuge [1,2] to examine the size of macromolecules. In this technique macromolecules are subjected to a sufficiently high centrifugal force (up to 250,000 $\times$ g) to effect their separation on the basis of size and shape, a process monitored by means of an optical system. A major outcome of this pioneering work for which Svedberg was awarded a Nobel Prize in 1926 was the demonstration that protein molecules were discrete entities rather than polymers with random chain length and sequence – the prevailing viewpoint at that time. The use of analytical ultracentrifugation for characterizing macromolecular assemblies has certainly been the subject of past reviews [3–5]; but a return to the topic is timely in view of developments in the field over the last decade.

A major focus of early ultracentrifugal studies was the characterization of protein migration in terms of a sedimentation coefficient (s), the ratio of the rate of migration ($\mathrm{d}r/\mathrm{d}t$) to the applied centrifugal field, the product of the square of angular velocity and radial distance from the centre of rotation ($\omega^2 r$). Although information on the translational diffusion coefficient (D) was potentially available from the extent of spreading of the migrating protein boundary, the determination of D from sedimentation velocity patterns had to await the development of an analysis that takes into account the boundary sharpening arising from negative concentration dependence of the sedimentation coefficient [6,7]. Attention was therefore directed towards the determination of sedimentation coefficient distributions from which the effects of diffusion were eliminated by their extrapolation to infinite time on the basis that spreading arising from

differences in s varies linearly with time whereas diffusional spreading is proportional to $\sqrt{t}$ [8,9].

The need for separate evaluation of s and D to determine molecular mass via the Svedberg equation can be avoided by operating the ultracentrifuge at lower speed to allow equilibrium attainment between centrifugal migration and the opposing diffusion phenomenon. However, its application to protein solutions was effectively precluded for thirty years by the length of time (weeks) required for equilibrium attainment. Fortunately, the realization that the duration of these sedimentation equilibrium experiments could be decreased to about 24 hours by shortening the length of the liquid column subjected to centrifugation from 1 cm to 3 mm or less [10] rendered practicable the assessment of molecular mass by this simpler and more accurate sedimentation equilibrium procedure.

During the course of these ultracentrifuge studies designed to characterize proteins in terms of size and homogeneity it became apparent that some protein solutions comprised a series of oligomeric states in rapid association equilibrium. Instead of exhibiting the negative s–c dependence observed for a single protein entity, these self-associating proteins were characterized by positive s–c dependence [11]. Because quantitative interpretation of this s–c dependence requires the assignment of magnitudes to the sedimentation coefficients of all participating oligomeric states [12], attention was diverted to the characterization of protein self-association by the emerging sedimentation equilibrium technique on the grounds of an integer relationship between the molecular masses of successive oligomeric states [13,14].

Interest in the use of analytical ultracentrifugation for the physicochemical characterization of proteins declined soon thereafter, but was rekindled by the production of new-generation analytical ultracentrifuges (the Beckman XL-A and XL-I instruments) towards the end of last century. By then the massive advances in computer technology had opened up the possibility of employing numerical simulation to solve the problems addressed by the earlier

analyses of sedimentation distributions. These developments led to a dramatic resurgence of activity in the analytical ultracentrifugation field that has entailed revitalization of the research endeavours begun some fifty years earlier. Unfortunately, the prerequisite for undertaking such studies of macromolecular interactions seems to have switched from a detailed understanding of the underlying thermodynamic and biophysical principles to a more technical requirement of knowledge and dexterity in the uploading and operation of readily available computer programs. Although sedimentation velocity may seem to be a more accurate procedure than sedimentation equilibrium [15] such a conclusion disregards the fact that the quantitative characterization of an interacting system is conditional upon the validity of assumptions about the magnitudes of sedimentation coefficients for putative product species as well the rates of species interconversion. The corresponding prerequisite for quantitative interpretation of sedimentation equilibrium distributions is knowledge of the molecular masses of the two reactants, which then allows the unequivocal assignment of a molecular mass to any putative product of the reversible interaction.

The resurgence of interest in the use of analytical ultracentrifugation for studying macromolecular complex formation has heralded a marked change in the reason for their study. Whereas interactions had previously been selected on the basis of their ability to exploit the virtues of ultracentrifugation for their investigation, studies have begun to emerge in which the actual biological system is the focus of interest. The major purpose of this review is to provide illustrations of the progress being made in the latter endeavour.

2. Quantitative description of sedimentation distributions

The migration of a single, noninteracting solute under the influence of a centrifugal field is described by the Lamm equation:

$$\left(\frac{\partial c}{\partial t}\right)_r = -\frac{1}{r}\frac{\partial}{\partial r}\left[r\left(cs\omega^2 r - D\left(\frac{\partial c}{\partial r}\right)_t\right)\right]_t \qquad (1)$$

where c is the weight concentration of solute at radial distance r, t is the time of centrifugation at angular velocity ω. s denotes the sedimentation coefficient and D the translational diffusion coefficient. Operation of an ultracentrifuge at high rotor speed leads to a situation wherein domination of the sedimentation term ($cs\omega^2 r$) gives rise to a migrating boundary that spreads with time because of an opposing diffusional flow in response to the resulting concentration gradient [the $-D(\partial c/\partial r)_t$ term]. Development of the typical *S*-shaped sedimentation velocity distributions is illustrated in Fig. 1. Although an exact analytical solution to this equation has not been found, it is amenable to numerical solution by freely available programs such as ULTRASCAN, SEDANAL, SEDFIT and SVEDBERG.

By diminishing the dominance of the sedimentation term a decrease in rotor speed increases the relative influence of the diffusion term – a situation of which advantage is taken in the sedimentation equilibrium variant of analytical ultracentrifugation. The selection of ω such that the opposing flows of comparable magnitude gives rise to distributions of the form shown in Fig. 2. Initially there is time dependence of the c–r distribution as the effects of sedimentation and diffusion come into play; but eventually the distribution becomes time-independent as the opposing flows self-cancel at all radial positions within the liquid column being subjected to ultracentrifugation. The effective attainment of sedimentation equilibrium is recognized by the essential overlay of distributions recorded (say) 4 hours apart in an experiment of 24 hours duration. Sedimentation equilibrium distributions assume one of two forms, depending on the rotor speed selected. In low-speed sedimentation equilibrium experiments [10] the speed is selected to generate a distribution in which the concentration is finite across the entire column length, whereas adoption of the high-speed sedimentation equilibrium option [17] gives rise to a

distribution containing a region with c essentially zero (Fig. 2). Analysis of sedimentation equilibrium distributions for an ideal, noninteracting solute is based on the expression

$$c(r) = c(r_F)\exp[M(1-\bar{v}\rho)\omega^2(r^2 - r_F^2)/(2RT)] \quad (2)$$

which describes the radial dependence of solute concentration in terms of that, $c(r_F)$, at a selected reference radial distance (r_F) and the buoyant molecular mass, $M(1-\bar{v}\rho)$, where $\bar{v}$ is the solute partial specific volume and ρ the solvent density: R is the universal gas constant and T the absolute temperature. Although a low-speed experiment has the potential to provide a larger [r, $c(r)$] data set than the corresponding experiment of meniscus-depletion design, that advantage is offset in Rayleigh interference records of the distribution by the fact that the concentration parameter monitored is the difference between $c(r)$ and the concentration at the air–liquid meniscus, $c(r_a)$: a means of ascertaining the solute concentration at the meniscus is thus required in low-speed runs in order to obtain a distribution in terms of absolute concentration. Programs such as ORIGIN, ULTRASCAN AND SEDFIT provide estimates of the buoyant molecular mass from sedimentation equilibrium distributions; and the program SEDNTERP affords a means of calculating the solute partial specific volume and buffer density – the parameters required for its conversion to a molecular mass.

3. Ultracentrifugal studies of macromolecular complex formation

As noted in the Introduction, most attention has been given to the development of methodology for the characterization of proteins and protein–protein interactions [18–21] as well as their protein–nucleic acid counterparts [22–25] by analytical ultracentrifugation. However attention has recently turned to the use of the technique as an analytical tool to assist with characterizing the complex assemblies that abound in biological systems. We now employ three such studies to illustrate the progress being made in those endeavours.

3.1. The cytoplasmic dynein complex

The dynein family of microtubule associated cytoskeletal motor proteins comprises axonemal dynein and cytoplasmic dynein (CyDn). Both dynein proteins contain one to three heavy chains with a molecular mass of about 530 kDa that consist of a 160 kDa N-terminal domain within which a number of accessory domains interact, and a 380 kDa motor domain at the C-terminus [26]. The cytoplasmic dynein can be further subdivided into CyDn1, a component of all cells containing microtubules, and CyDn2, which is only present around cilia and flagella. The CyDn1 (~1.4 MDa) is a homodimer composed of two heavy chains (~530 kDa, containing three AAA+ ATPase domains) as well as a number of associated domains including an intermediate chain (~75 kDa), a light intermediate chain (~55 kDa), a T-complex testis-specific protein 1 (Tctex1, ~13 kDa), Roadblock protein (~11 kDa), and three light chains (~8 kDa) [27–30]. CyDn1 is a major player affecting vital cellular activities such as a molecular motor involved in transportation of cellular components (e.g. Golgi, peroxisomes, endosomes), chromosomal segregation, mitosis as well as viral infection [31–35].

In order to investigate the assembly of CyDn1 in solution, Trokter and colleagues [36] expressed dynein proteins and their interacting partners in bacteria (light chain 8 – LC8, light chain - LC, light intermediate chain – LIC2, RB1 and TcTex1) and insect (heavy chain - CDHC and intermediate chain – IC1) hosts, after which affinity and size exclusion chromatography were used as purification steps. A complex of heavy chain, LIC2 and IC1 was first purified by means of an affinity tag attached to heavy chain – a step followed by the formulation of CyDn1 assembly and its purification by size exclusion chromatography. The 380 kDa motor region of heavy chain was also purified by affinity and size exclusion chromatography. Individual proteins as well as their complexes were then subjected to ultracentrifugation at 30,000 to

40,000 rpm and 20 ˚C; and the resulting sedimentation velocity distributions were analysed by means of the g*(s) method implemented in the DCDT+ program (Version 2.3.2) [37,38].

The entire CyDn1 complex containing heavy chain, LC1, LIC2, Tctex1, LC8 and RB1 components yielded a sedimentation coefficient of 22 S. A molecular mass estimate was then determined by combining this value for s with the hydrodynamic radius (R_h) of 16 nm [36] obtained by size exclusion chromatography in the expression [39]

$$M = 6\pi N_A \eta R_h s/(1-v\rho) \qquad [3]$$

where N_A is Avogadro's number and η the solvent viscosity. The relatively good agreement between the resulting estimate of 1.56 MDa and the sequence molecular mass of 1.4 MDa was taken to signify the successful reconstitution of the human CyDn1 complex – a stance reinforced by the use of SDS-PAGE to detect the presence of all components in the complex.

In order to establish whether the dimeric nature of the heavy chain in the dynein1 complex (a feature confirmed by electron microscopy) was an intrinsic property of the heavy chain itself or a consequence of its interacting partners, attempts were made to purify the heavy chain alone; but this endeavour was plagued by aggregation/insolubility problems. An increase in buffer ionic strength to 0.3 M increased the solubility sufficiently to allow investigation of the solution characteristics by sedimentation velocity and size-exclusion chromatography. Combination of the sedimentation coefficient of 16 S for the major peak of a distribution exhibiting a broad faster-migrating tail with the corresponding estimate of 10.1 nm for R_h yielded a molecular mass of 705 kDa, which is considerably higher than the sequence value of 563 kDa. Whereas Trokter et al. [36] considered the heavy chain alone to be monomeric, the high estimate of M and the asymmetric form of the sedimentation coefficient distribution leave open the possibility of the coexistence of monomer in association equilibrium with higher

oligomeric states that exhibit lower solubility. Further comment on this possibility is precluded by an absence of sedimentation velocity distributions for a range of heavy chain concentrations.

Corresponding studies of the 380 kDa motor domain of the heavy chain yielded a highly soluble protein with a sedimentation coefficient of 12 S and a hydrodynamic radius of 8.6 nm, and hence an estimate of 456 kDa for M that was considered to signify a monomeric state for this C-terminal domain of dynein. The lower solubility of the entire heavy chain must therefore be attributed to the N-terminal region of dynein1. Although more studies are required, the application of analytical ultracentrifugation in conjunction with other solution procedures clearly has the potential to provide information on the macromolecular nature of cytoplasmic dynein in its native state.

3.2. ERK2 self-interaction

ERK2, also known as mitogen-activated protein kinase 1 (MAPK1) is a Ser/Thr kinase that is involved in Ras-Raf-MEK-ERK signal transduction pathways [40]. These pathways further regulate a number of cellular processes such as cell adhesion, differentiation, migration, survival, cell cycle progression and transcription [41]. The MKK1 and MKK2 proteins (mitogen-activated protein kinase kinases 1 and 2) are activated by Raf kinases, which further activate the ERK1 and ERK2 that target downstream signalling proteins to mediate a variety of cellular functions [42,43]. There has been conflicting evidence in the literature about whether ERK2 is monomeric or dimeric in solution. Although the high-resolution structure of His-tagged ERK2 was monomeric, a potential site for dimerization was identified on its surface [44]; and His-tagged ERK2 was also demonstrated to self-associate in solution regardless of its phosphorylation state [44] – a finding in conflict with an earlier study that demonstrated phosphorylation-dependent self-association [45]. This dimerization of His-tagged ERK2 was

considered to require the presence of $MgCl_2$ and $CaCl_2$ because of its monomeric nature in the presence of EDTA/EGTA [46,47].

To investigate whether the His-tag could be responsible for the self-association, Kaoud et al. [48] prepared ERK2 with the His-tag removed. His-tagged ERK2 was again expressed in bacterial cells and purified by affinity chromatography on a N-chelated Sepharose column. After removal of the His-tag by enzymatic cleavage, the ERK2 was subjected to anion exchange chromatography and then activated using MKK1 before final purification by hydrophobic interaction chromatography [48]. SEC-MALLS experiments were performed on ERK2 in the presence and absence of $MgCl_2$ (10 mM). The same conditions were also used to determine the translational diffusion coefficient by dynamic light scattering; and also to characterize ERK2 by sedimentation velocity and equilibrium experiments, the concentration distributions from which were analysed with the UltraScan 9.9 software [49].

SEC-MALLS experiments on activated ERK2 (~ 9.0 μM) yielded a molecular mass of 42 kDa, which matches the sequence molecular weight of 41.71 kDa and was unaffected by the presence of divalent cations. A similar conclusion emerged from the dynamic light scattering studies in that the diffusion coefficient obtained at multiple concentrations was unaffected by the presence of $MgCl_2$ or $CaCl_2$. On the other hand a light scattering study confirmed the earlier finding [44] that activated (phosphorylated) His-tagged ERK2 undergoes dimerization – irrespective of the presence or absence of $MgCl_2$.

The same conclusions emerged from studies of the activated ERK2 by analytical ultracentrifugation. Analysis of the concentration distributions from a sedimentation velocity experiment on a 0.63 mg/mL solution by the Van Holde and Weischet procedure [50] as upgraded by Demeler and Van Holde [51] and implemented in ULTRASCAN [49] yielded a single peak with sedimentation coefficient ($s_{20,w}$) of 3.2 S. Combination of this value and the calculated partial specific volume of 0.743 mg/mL with the hydrodynamic radius of 2.8 nm [48]

in Equation (3) also signifies a molecular mass of 40 kDa and hence a monomeric state for activated ERK2. Finally, the global application of Equation (2) to sedimentation equilibrium distributions obtained by centrifuging three ERK2 solutions (initial concentrations between 4.8 and 11.2 μM) at two rotor speeds yielded a molecular mass estimate of 40.18 (± 0.2) kDa – a value unaffected by the presence of $MgCl_2$. Although it could be argued that a larger concentration range could have been used to eliminate completely the possibility of weak dimerization, those sedimentation equilibrium results provide unequivocal evidence for the existence of activated ERK2 as a monomer in its native (unmodified) state.

In summary, Kaoud et al [48] have employed a variety of physicochemical techniques to show convincingly that the earlier reports of ERK2 dimerization in solution [44–47] were misleading in that the results referred to the self-association of a chemically modified (His-tagged) form of the enzyme. Inasmuch as the reported high-resolution structure [44] also refers to the His-tagged enzyme its relevance to that of unmodified ERK2 may well require further scrutiny. However, there is now agreement between solution and crystallographic studies about the oligomeric state of ERK2.

3.3. The terminal catalytic complex in selenocysteine synthesis

O-phosphoseryl-tRNA:selenocysteinyl-tRNA synthase (SepSecS) is a pyridoxal 5-phosphate (PLP) dependent enzyme that converts O-phospho-L-seryl-tRNA^{Sec} and selenophosphate into L-selenocysteinyl-tRNA^{Sec} in the second step of a pathway involving the formation of selenocysteinyl-tRNA^{Sec} from L-seryl-tRNA^{Sec} substrate in eukaryotes and archea [52]. The SepSecS enzyme has been shown to form a stable tetramer; and the high-resolution structure of SepSecS in complex with tRNA^{Sec} has signified that only two of the four binding sites of the tetrameric enzyme are occupied by molecules of tRNA^{Sec} [53].

In order to examine whether the solution conformation and interactions of SepSecS with tRNA^{Sec} parallel those observed in the high-resolution structure, French and co-workers [54] performed a series of sedimentation velocity, SEC-MALLS (size exclusion chromatography coupled with multiangle laser light scattering) and SAXS (small angle X-ray scattering) experiments. The SepSecS protein was expressed in a bacterial host and purified using affinity tag followed by analytical SEC. The tRNA^{Sec} was prepared using *in vitro* transcription followed by purification to homogeneity using analytical SEC. Sedimentation velocity experiments were performed at 35,000 rpm and 20 ˚C; and the concentration distributions were analysed with the Ultrascan III software [49]. In experiments on the individual reactants the concentrations of tRNA^{Sec} and SepSecS were 0.28 mg/mL and 1.5 mg/mL respectively, whereas experiments on mixtures contained a fixed concentration (23 μg/mL of tRNA^{Sec} and a range of SepSecS concentrations to give molar ratios (total ligand/total enzyme) of 2:1, 4:1, 6:1 and 8:1. The SEC-MALLS and SAXS experiments also used similar concentrations for individual species and the same molar ratios for mixtures thereof. These experiments were interpreted in terms of stoichiometric interaction between tRNA^{Sec} and SepSecS on the grounds that the intrinsic dissociation constant (*Kd*) of 0.078 μM obtained from fluorescence quenching measurements under similar conditions ensured stability of the complexes [54]. However, substitution of a

value of 0.9 for the fractional saturation f in the expression $f = [tRNA^{Sec}]/(K_d + [tRNA^{Sec}])$ reveals that a free ligand concentration of 0.7 μM would be required to achieve 90% saturation of the SepSecS sites in the sedimentation velocity experiments with a total $tRNA^{Sec}$ concentration of about 0.8 μM. A mixture of reactants and complexes in association equilibrium is thus the predicted situation.

The Van Holde–Weischet distributions for the two individual reactants exhibited the step-function increase in concentration indicative of single species and respective sedimentation coefficients of 4.3 and about 9 S for $tRNA^{Sec}$ and SepSecS (Fig. 3). For the mixture with a 2:1 molar excess of tRNASec the major feature of the concentration distribution is a spread boundary with a pronounced concentration increase at 10 S (Fig. 3). Although the latter sedimentation coefficient was identified with that of a stable complex [54], the form of the distribution renders more appropriate its interpretation in terms of a reaction boundary across which the concentrations of the two reactants as well as the complex(es) vary [55]. Indeed, an early goal of determining the form of diffusion-free sedimentation profiles [56] was the conversion of experimental distributions into forms commensurate with their Gilbert counterparts. The fact that increasing the molar ratio of $tRNA^{Sec}$ to SepSecS increased the proportion of the slow boundary relative to that of the faster-migrating reaction boundary (Fig. 3) merely reflects the fact that the molar ratio increase was effected at the expense of enzyme concentration. Finally, the termination of the reaction boundary at about 10 S is consistent with the binding of $tRNA^{Sec}$ to two equivalent and independent sites on SepSecS inasmuch as that sedimentation coefficient is smaller than the value of 11.8 S that we have calculated from the crystal structure of the complex by means of the HYDROPRO program [57].

Such interpretation of the sedimentation velocity results is completely consistent with the SEC-MALLS elution profiles (Fig. 2A of [54]); and also accounts for the fact that molecular mass measurements across the eluted reaction zone yield values that are intermediate between

those of the 1:1 and 1:2 SepSecS–tRNA^{Sec} complexes (Fig. 2B of [54]). Failure to observe a molecular mass increase in elution profiles reflecting higher molar tRNA^{Sec}:SepSecS ratios precludes the attempted rationalization in terms of an apparent proportion of stable 1:1 and 2:1 complexes [54].

The results obtained from size-exclusion chromatography experiments in which the eluate was monitored by SAXS measurements [54] provide additional support for consideration of the solution behaviour of tRNA^{Sec}–SepSecS mixtures in terms of equivalent and independent binding to two sites on the tetrameric protein. Complex formation was indicated by the increase in the radius of gyration (R_g) from 4.3 nm for SepSecS to 4.8–4.9 nm in the faster-eluting zone for tRNA^{Sec}–SepSecS mixtures; and a reaction stoichiometry greater than 2 was rendered unlikely by the use of the CRYSOL program [58] to calculate a value of 5.16 nm for R_g from the crystal structure coordinates for the 2:1 tRNA^{Sec}–SepSecS complex.

In summary, the physicochemical procedures adopted by French et al. [54] to examine complex formation between tRNA^{Sec} and SepSecS have yielded no evidence that questions the existence of only two binding sites for ligand on the terameric SepSecS protein − the situation deduced from X-ray crystallographic studies [53]. It would therefore appear that the solution behaviour of this system is also consistent with the binding of a tRNA^{Sec} molecule across two protein subunits that is observed in the high resolution crystal structure.

4. Concluding remarks

The three illustrative examples of the use of ultracentrifugation to examine the solution properties of biologically important protein complexes have served to demonstrate different ways in which the technique can contribute to our understanding of macromolecular assemblies.

(i) In the first a combination of sedimentation velocity and size-exclusion chromatography experiments was used to establish the successful reconstitution of the CyDn1 complex; and also to decipher whether the dimeric nature of the heavy chain component within that complex was a intrinsic property of the heavy chain or a consequence of its prior interaction with other components of the complex – a question that remains unresolved by the information currently available.

(ii) The role of physicochemical characterization in studies of the mitogen-activated protein kinase system (ERK2) was to settle a dispute about its oligomeric state. Whereas X-ray crystallography had yielded a monomeric structure, the ERK2 preparation underwent self-association in solution. However, this self-association reflected the use of a His-tagged ERK2 preparation rather than the native enzyme with the His-tag removed. This example again highlights the dangers of disregarding the possible consequences of even slight chemical modification on the physicochemical properties of a protein – a problem to which attention was drawn many years ago in a comparable situation where a fluorescein probe was used to facilitate the detection of interactions between glycolytic enzymes by fluorescence polarization measurements [59,60].

(iii) In the third example sedimentation velocity experiments were again used in conjunction with size-exclusion chromatography to determine the compatibility of the solution behaviour of $tRNA^{Sec}$–SepSecS mixtures with the crystal structure of the saturated enzyme-ligand complex, which only contained two $tRNA^{Sec}$ molecules on the tetrameric enzyme. Whereas the original interpretation of the results was based on stoichiometric complex formation, the results are considered to find more logical rationalization in terms of reversible interaction between $tRNA^{Sec}$ and two equivalent and independent sites on the tetrameric SepSecS. As well as establishing consistency of the solution behaviour with the basic tenets of the crystal structure, this reinterpretation of the data has stressed the valuable role that solution

studies can offer as a means of establishing whether interactions are stoichiometric or in a state of reversible association equilibrium.

In conclusion, the ultimate goal of structural biologists is to determine a high-resolution three-dimensional structure of a protein complex in order to identify the contributing interactions at a submolecular level: X-ray crystallography and NMR undoubtedly reign supreme for that purpose. Nevertheless, physicochemical procedures such as analytical ultracentrifugation, size-exclusion chromatography, and light scattering (static, dynamic and small-angle) have vital roles to play before the availability of a detailed three-dimensional structure, as well as in the identification of conditions conducive to crystallization. Their role is not terminated by the availability of that structure because they then afford the means of verifying its relevance to the situation prevailing in solution. In that regard the sedimentation equilibrium and sedimentation velocity variants of analytical ultracentrifugation provide powerful methods for characterizing protein–protein interactions, not only in terms of reaction stoichiometry (information also provided by the high-resolution structure) but also the equilibrium constant(s) governing the interaction(s). In other words, solution methods afford a potential means of characterizing the composition of an interacting mixture and hence the extent to which reaction occurs under the prevailing conditions (pH, ionic strength, and total reactant concentrations) – an important consideration from the physiological/pharmacological viewpoint.

Acknowledgements

TRP is supported by the Marie Skłodowska-Curie Fellowship.

References

[1] T. Svedberg, H. Rinde, The ultracentrifuge: a new instrument for the determination of size and distribution of size of particle in amiscroscopic colloids. J. Am. Chem. Soc. 46 (1924) 2677–2693.

[2] T. Svedberg, K.O. Pedersen, The Ultracentrifuge, Clarendon Press, Oxford, UK, 1940.

[3] T.M. Laue, W.F. Stafford, Modern applications of analytical ultracentrifugation. Annu. Rev. Biophys. Biomol. Struct. 28 (1999) 75–100.

[4] J. Lebowitz, M.S. Lewis, P. Schuck, Ultracentrifugation in protein science: a tutorial. Protein Sci. 11 (2002) 2067–2079.

[5] G.J. Howlett, A.P. Minton, G. Rivas, Analytical ultracentrifugation for the study of protein association and assembly. Curr. Opin. Chem. Biol. 10 (2006) 430–436.

[6] H. Fujita, Evaluation of diffusion coefficients from sedimentation velocity measurements. J. Phys. Chem. 63 (1959) 1092–1095.

[7] H. Fujita, Mathematical Theory of Sedimentation Analysis, Academic Press, New York, 1962.

[8] J.W. Williams, R.L. Baldwin, W.M. Saunders, P.G. Squire, Boundary spreading in sedimentation velocity experiments. I. The enzymatic degradation of serum globulins. J. Am. Chem. Soc. 74 (1952) 1542–1548.

[9] R.L. Baldwin, Boundary spreading in sedimentation velocity experiments. III. Effects of diffusion on the measurement of heterogeneity when concentration dependence is absent. J. Phys. Chem. 58 (1954) 1081–1086.

[10] K.E. Van Holde, R.L. Baldwin, Rapid attainment of sedimentation equilibrium. J. Phys. Chem. 62 (1958) 734–743.

[11] G.W. Schwert, The molecular size and shape of the pancreatic proteases: I. Sedimentation studies on chymotrypsinogen and on α- and γ-chymotrypsin. J. Biol. Chem. 179 (1949) 655–664.

[12] G.A. Gilbert, Sedimentation and electrophoresis of interacting substances. III. Sedimentation of a reversibly aggregating substance with concentration dependent sedimentation coefficients. Proc. R. Soc. (London) A276 (1963) 354–366.

[13] M.S.N. Rao, G. Kegeles, An ultracentrifuge study of the polymerization of α-chymotrypsin. J. Am. Chem. Soc. 80 (1958) 5724–5729.

[14] E.T. Adams, H. Fujita, Sedimentation equilibrium in reacting systems. In: J.W. Williams (Ed.), Ultracentrifugal Analysis in Theory and Experiment, Academic Press, New York, 1963, pp. 119–129.

[15] B. Demeler, E. Brookes, R. Wang, V. Scherf, C.A. Kim, Characterization of reversible association by sedimentation velocity with Ultrascan. Macromol. Biosci. 10 (2010) 775–782.

[16] T.R. Patel, D.R. Picout, S.B. Ross-Murphy, S.E. Harding, Pressure cell assisted solution characterization of galactomannans. 3. Application of analytical ultracentrifugation techniques. Biomacromolecules 7 (2006) 3513-20.

[17] D.A. Yphantis, D.A. (1963). Equilibrium ultracentrifugation in dilute solutions. Biochemistry 3 (1963) 297–317.

[18] L. Shapiro, J.P. Doyle, P. Hensley, D.R. Colman, W.A. Hendrickson, Crystal structure of the ectracellular domain from Po, the major structural protein of peripheral nerve myelin, Neuron 17 (1996) 435–439.

[19] R.J. Gilbert, J. Rossjohn, M.W. Parker, R.K. Tweten, P.J. Morgan, T.J. Mitchell, N. Errington, A.J. Rowe, P.W. Andrew, O. Byron, Self-interaction of pneumolysin, the pore-forming toxin of *Streptococcus pneumoniae*. J. Mol. Biol. 284 (1998) 1223–1237.

[20] R. Barry, S. Moore, A. Alonso, J. Ausio, J.T. Buckley, The channel-forming protein proaerolysin remains a dimer at low concentrations in solution. J. Biol. Chem. 276 (2001) 551–554.

[21] J.L. Whittingham, D.J. Scott, K. Chance, A. Wilson, J. Finch, J. Brange, G.G. Dodson, Insulin at pH 2: Structural analysis of the conditions promoting insulin fibre formation. J. Mol. Biol. 318 (2002) 479–490.

[22] S.J. Grieve, A.F. Lins, P. von Hippel, Assembly of an RNA–protein complex: Binding of NusB and NUsE (S10) proteins to boxA RNA nucleates the formation of the antitermination complex involved in controlling rRNA transcription in *Escherichia coli*. J. Biol. Chem. 280 (2005) 36397–36408.

[23] Z. Pietras, S.W. Hardwick, S. Swiezewski, B.F. Luisi, Potential regulatory interactions of *Escherichia coli* RraA protein with DEAD-box helicases. J. Biol. Chem. 288 (2013) 31919–31929.

[24] R.M. Scheiba, Al de Opakua, A. Diaz-Quintana, I. Cruz-Gallardo, L.A. Martinez-Cruz, M.L. Martinez-Chantar, F.J. Blanco, I. Diaz-Moreno, The C-terminal RNA binding motif of HuR is a multi-functional domain leading to HuR and binding to U-rich RNA targets. RNA Biol. 11 (2014) 1250–1261.

[25] F.N. Musayev, F. Zarate-Perez, C. Bishop, J.W. Burgner II, C.R. Escalante, Structural insights into the assembly of the adeno-associated virus tupe 2 Rep68 protein on the integration site AAVS1. J. Biol. Chem. (in press).

[26] P. Hook, R.B. Vallee, The dynein family at a glance. J. Cell Sci. 119 (2006) 4369–4371.

[27] R.B. Vallee, J.S. Wall, B.M. Paschal, H.S. Shpetner, Microtubule-associated protein 1C from brain is a two-headed cytosolic dynein. Nature 332 (1988) 561–563.

[28] S.M. King, E. Barbarese, J.F. Dillman, R.S. Patel-King, J.H. Carson, K.K. Pfister, Brain cytoplasmic and flagellar outer arm dyneins share a highly conserved Mr 8,000 light chain. J. Biol. Chem. 271 (1996) 19358–19366.

[29] S.M. King, J.F. Dillman, S.E. Benashski, R.J. Lye, R.S. Patel-King, K.K. Pfister, The mouse t-complex-encoded protein Tctex-1 is a light chain of brain cytoplasmic dynein. J. Biol. Chem. 271 (1996) 32281–32287.

[30] K. Nikulina, R.S. Patel-King, S. Takebe, K.K. Pfister, S.M. King, The Roadblock light chains are ubiquitous components of cytoplasmic dynein that form homo- and heterodimers. Cell Motil. Cytoskeleton 57 (2004) 233–245.

[31] E.L. Holzbaur, R.B. Vallee, Dyneins: molecular structure and cellular function. Annu. Rev. Cell Biol. 10 (1994) 339–372.

[32] W. Steffen, S. Karki, K.T. Vaughan, R.B. Vallee, E.L. Holzbaur, D.G. Weiss, S.A. Kuznetsov, The involvement of the intermediate chain of cytoplasmic dynein in binding the motor complex to membranous organelles of Xenopus oocytes. Mol. Biol. Cell (1997) 2077–2088.

[33] A. Harada, Y. Takei, Y. Kanai, Y. Tanaka, S. Nonaka, N. Hirokawa, Golgi vesiculation and lysosome dispersion in cells lacking cytoplasmic dynein. J. Cell Biol. 141 (1998) 51–59.

[34] C. Kural, H. Kim, S. Syed, G. Goshima, V.I. Gelfand, P.R. Selvin, Kinesin and dynein move a peroxisome in vivo: a tug-of-war or coordinated movement? Science 308 (2005) 1469–1472.

[35] R.J. Diefenbach, M. Miranda-Saksena, M.W. Douglas, A.L. Cunningham, Transport and egress of herpes simplex virus in neurons. Rev. Med. Virol. 18 (2008) 35–51.

[36] M. Trokter, N. Mucke, T. Surrey, Reconstitution of the human cytoplasmic dynein complex. Proc. Natl. Acad. Sci. USA 109 (2012) 20895–20900.

[37] W.F. Stafford, Boundary analysis in sedimentation transport experiments: a procedure for obtaining sedimentation coefficient distributions using the time derivative of the concentration profile. Anal. Biochem. 203 (1992) 295–301.

[38] J.S. Philo, Improved methods for fitting sedimentation coefficient distributions derived by time-derivative techniques. Anal. Biochem. 354 (2006) 238–246.

[39] T.R. Patel, D. Nikodemus, T.M.D. Besong, R. Reuten, M. Meier, S.E. Harding, D.J. Winzor, M. Koch, J. Stetefeld, Biophysical analysis of a lethal laminin alpha-1 mutation reveals altered self-interaction. Matrix Biol. (in press).

[40] I. Wortzel, R. Seger, The ERK Cascade: Distinct Functions within Various Subcellular Organelles. Genes Cancer 2 (2011) 195–209.

[41] R. Roskoski, ERK1/2 MAP kinases: structure, function, and regulation. Pharmacol. Res. 66 (2012) 105–143.

[42] C.F. Zheng, K.L. Guan, Cloning and characterization of two distinct human extracellular signal-regulated kinase activator kinases, MEK1 and MEK2. J. Biol. Chem. 268 (1993) 11435–11439.

[43] J.E. Ferrell, Jr., R.R. Bhatt, Mechanistic studies of the dual phosphorylation of mitogen-activated protein kinase. J. Biol. Chem. 272 (1997) 19008–19016.

[44] A.V. Khokhlatchev, B. Canagarajah, J. Wilsbacher, M. Robinson, M. Atkinson, E. Goldsmith, M.H. Cobb, Phosphorylation of the MAP kinase ERK2 promotes its homodimerization and nuclear translocation. Cell 93 (1998) 605–615.

[45] B.J. Canagarajah, A. Khokhlatchev, M.H. Cobb, E.J. Goldsmith, Activation mechanism of the MAP kinase ERK2 by dual phosphorylation. Cell 90 (1997) 859–869.

[46] K.A. Callaway, M.A. Rainey, A.F. Riggs, O. Abramczyk, K.N. Dalby, Properties and regulation of a transiently assembled ERK2.Ets-1 signaling complex. Biochemistry 45 (2006) 13719–13733.

[47] J.L. Wilsbacher, Y.C. Juang, A.V. Khokhlatchev, E. Gallagher, D. Binns, E.J. Goldsmith, M.H. Cobb, Characterization of mitogen-activated protein kinase (MAPK) dimers. Biochemistry 45 (2006) 13175–13182.

[48] T.S. Kaoud, A.K. Devkota, R. Harris, M.S. Rana, O. Abramczyk, M. Warthaka, S. Lee, M.E. Girvin, A.F. Riggs, K.N. Dalby, Activated ERK2 is a monomer in vitro with or without divalent cations and when complexed to the cytoplasmic scaffold PEA-15. Biochemistry 50 (2011) 4568–4578.

[49] B. Demeler, B. UltraScan – a comprehensive data analysis software package for fnalytical ultracentrifugation experiments. In: D.J. Scott, S.E. Harding,

A.J. Rowe, (Eds.), Analytical Ultracentrifugation: Techniques and Methods, Royal Society of Chemistry, Cambridge, UK, 2005, pp. 210–229

[50] K.E. Van Holde, W.O. Weischet, Boundary analysis of sedimentation velocity experiments with monodisperse and paucidisperse solutes..Biopolymers 17 (1978) 1387–1403.

[51] B. Demeler, K.E. Van Holde, Sedimentation velocity analysis of highly heterogeneous systems. Anal. Biochem. 335 (2004) 279–288.

[52] J. Yuan, S. Palioura, J.C. Salazar, D. Su, P. O'Donoghue, M.J. Hohn, A.M. Cardoso, W.B. Whitman, D. Soll, RNA-dependent conversion of phosphoserine forms selenocysteine in eukaryotes and archaea. Proc. Natl. Acad. Sci. USA 103 (2006) 18923–18927.

[53] S. Palioura, R.L. Sherrer, T.A. Steitz, D. Söll, M. Simonović, The human SepSecS-tRNASec complex reveals the mechanism of selenocysteine formation. Science 325 (2009) 321–325.

[54] R.L. French, N. Gupta, P.R. Copeland, M. Simonovic, Structural asymmetry of the terminal catalytic complex in selenocysteine synthesis. J. Biol. Chem. 289 (2014) 28783–28794.

[55] G. A. Gilbert, R.C.L. Jenkins, Sedimentation and electrophoresis of interacting substances. II. Idealized boundary shape for two substances interacting reversibly. Proc. R. Soc. (London) A253 (1959) 420–437.

[56] D.J. Winzor, R. Tellam, L.W. Nichol, Determining the asymptotic shapes of sedimentation velocity distributions for reversing polymerizing solutes. Arch. Biochem. Biophys. 178 (1977) 327–332.

[57] J. Garcia De La Torre, M.L. Huertas, B. Carrasco, Calculation of hydrodynamic properties of globular proteins from their atomic-level structure. Biophys. J. 78 (2000) 719–730.

[58] D. Svergun, C. Barberato, M.J.H. Koch, CRYSOL: a program to evaluate X-ray solution scattering of biological macromolecules from atomic coordinates. *J. Appl. Crystallogr*. 28 (1995) 768–773.

[59] J. Ovádi, T. Keleti, C. Salerno, P. Fasella, Physicochemical evidence for the interaction between alsolase and glyceraldehyde-3-phosphate dehydrogenase. Eur. J. Biochem. 90 (1978) 499–503.

[60] C.J. Masters, D.J. Winzor, Physicochemical evidence against the concept of an interaction between aldolase and glyceraldehyde-3-phosphate dehydrogenase. Arch. Biochem. Biophys. 209 (1981) 185–190.

LEGENDS TO FIGURES

Fig. 1. Concentration distributions recorded by the Rayleigh interference optical system in a sedimentation velocity experiment on a macromolecular solute. The solid vertical line denotes the radial position of the air–sample meniscus, and the dashed line the corresponding position of the air–solvent meniscus in the reference channel of the double-sector cell. Accumulation of solute at the cell base accounts for the dramatic concentration increases at the right-hand extreme of the distributions. (Data taken from Fig. 2 of [16].)

Fig. 2. Illustrative sedimentation equilibrium distributions for a 3-mm liquid column (r = 6.85–7.15 cm) of a 45 kDa protein subjected to centrifugation at 10,000 and 30,000 rpm: the horizontal data reflect the initial distribution for the low speed (LS) run, and the other (HS) a distribution reflecting meniscus depletion at the higher rotor speed.

Fig. 3. Asymptotic (diffusion-free) sedimentation velocity distributions for $tRNA^{Sec}$ and SepSecS as well as for mixtures thereof in the indicated $tRNA^{Sec}$:SepSecS molar ratios. The stepwise forms of the distributions for the individual reactants signify their existence as stable species in solution, whereas the spread forms of those for mixtures indicate the existence of reversible complex formation between the two reactants. (Data taken from Fig. 1A of [54].)